

# SCUBA polarisation observations of the magnetic fields in the prestellar cores L1498 and L1517B

J. M. Kirk<sup>1,2</sup>, D. Ward-Thompson<sup>1,3</sup>, R. M. Crutcher<sup>2</sup>

<sup>1</sup>*School of Physics and Astronomy, Cardiff University, 5 The Parade, Cardiff, CF24 3YB*

<sup>2</sup>*Department of Astronomy, University of Illinois, 1002 West Green Street, Urbana, Illinois, IL61801, USA*

<sup>3</sup>*Observatoire de Bordeaux, 2 rue de l'Observatoire, 33270 Floirac, France*

Accepted 2006 March ?; received 2006 March 24; in original form 2006 January 17.

## ABSTRACT

We have mapped linearly polarized dust emission from the prestellar cores L1498 and L1517B with the James Clerk Maxwell Telescope (JCMT) using the Submillimetre Common User Bolometer Array (SCUBA) and its polarimeter (SCUBAPOL) at a wavelength of 850  $\mu$ m. We use these measurements to determine the plane-of-sky magnetic field orientation in the cores. In L1498 we see a magnetic field across the peak of the core that lies at an offset of  $\sim 19^\circ \pm 12^\circ$  to the short axis of the core. This is similar to the offsets seen in previous observations of prestellar cores. To the southeast of the peak, in the filamentary tail of the core, we see that the magnetic field has rotated to lie almost parallel to the long axis of the filament. We hypothesise that the field in the core may have decoupled from the field in the filament that connects the core to the rest of the cloud. We use the Chandrasekhar-Fermi (CF) method to measure the plane-of-sky field strength in the core of L1498 to be  $\sim 10 \pm 7 \mu$ G.

In L1517B we see a more gradual turn in the field direction from the northern part of the core to the south. This appears to follow a twist in the filament in which the core is buried, with the field staying at a roughly constant  $\sim 25^\circ \pm 6^\circ$  offset to the short axis of the filament, consistent with previous observations of prestellar cores. Hence these two clouds in an apparently similar evolutionary state, that exhibit similar masses, morphologies and densities, have very different magnetic field configurations. We again use the CF method and calculate the magnetic field strength in L1517B to be  $\sim 30 \pm 10 \mu$ G. Both cores appear to be roughly virialised. Comparison with our previous work on somewhat denser cores shows that, for the denser cores, thermal and non-thermal (including magnetic) support are approximately equal, while for the lower density cores studied here, thermal support dominates.

**Key words:** ISM: clouds – ISM: individual (L1498, L1517B) – ISM: magnetic fields – polarization – stars:formation

## 1 INTRODUCTION

The exact manner in which stars form is still a matter of debate. One important aspect of this debate centres around the morphology and magnitude of the magnetic field within molecular clouds and the magnitude of its effect on the star formation process. Observations of the magnetic field before protostellar collapse are necessary to address this question, ideally in a sample of molecular clouds that do not contain protostars but are on the verge of protostellar collapse.

Myers and co-workers developed a catalogue of dense molecular cores within dark clouds, which they observed in CO and later in ammonia (see: Benson & Myers 1989, and references therein). Beichman et al. (1986) cross-referenced the Myers ammonia catalogue with the IRAS point source

catalogue and identified starless cores as those that had not yet formed an embedded protostar. Ward-Thompson et al. (1994) observed the submillimetre continuum emission from starless cores and identified a subset of starless cores called prestellar (formerly pre-protostellar) cores that are thought to be about to form a protostar.

Kirk, Ward-Thompson & André (2005, hereafter KWA) observed a sample of 52 candidate prestellar cores with the Submillimetre Common User Bolometer Array (SCUBA) camera on the James Clerk Maxwell Telescope (JCMT). Twenty-nine of the cores were detected and were separated into ‘bright’ and ‘intermediate’ groups based on their 850- $\mu$ m peak flux densities. The bright cores were seen to be more centrally condensed. Following the method of Jessop & Ward-Thompson (2001), KWA showed that

## 2 Kirk, Ward-Thompson & Crutcher

the estimated lifetimes of the two groups were consistent with them being part of an evolutionary sequence.

Ward-Thompson et al. (2000) presented the first observations of the magnetic field geometry from prestellar cores when they mapped L183, L1544 and L43 with the SCUBA polarimeter. Their maps showed relatively smooth and uniform magnetic fields over the central core regions that were at an angle of approximately  $30^\circ$  to the projected minor axis of the cores. Crutcher et al. (2004) used the Ward-Thompson et al. (2000) data to estimate the strength of the magnetic field in the plane of the sky using an effect first suggested by Chandrasekhar & Fermi (1953, hereafter CF).

CF postulated that when the magnetic field is frozen to the matter, turbulent motions will cause local perturbations in a uniform magnetic field. These perturbations to the magnetic field should manifest themselves as a random scatter superimposed on an otherwise regularly oriented magnetic field pattern. If the magnitude of the random component of the dispersion,  $\delta\phi$ , and the turbulent motion,  $\delta V_{NT}$ , are known then CF showed that it is possible to infer the strength of the uniform plane-of-sky field  $B_{pos}$  in a medium of density  $\rho$ , such that:

$$B_{pos} = Q \sqrt{4\pi\rho} \frac{\delta V_{NT}}{\delta\phi} \approx 9.3 \sqrt{n(H_2)} \frac{\Delta V_{NT}}{\delta\phi} \mu G, \quad (1)$$

where  $\rho = mn(H_2)$ ,  $m$  is the mean particle mass,  $n(H_2)$  is the volume number density and  $\Delta V_{NT} = \delta V_{NT} \sqrt{8 \ln 2}$  is the full-width at half maximum (FWHM) of the non-thermal, or turbulent, linewidth.  $Q$  is a calibration factor, fixed by comparison with simulations, for which we follow Crutcher et al. (2004) in adopting a value of 0.5.

A crucial parameter in the study of magnetically influenced star formation is  $M/\Phi$ , which is the ratio of the mass to the magnetic flux and is normally expressed as  $\lambda$ , the ratio of the observed mass-to-flux ratio  $(M/\Phi)_{obs}$  to the critical mass-to-flux ratio  $(M/\Phi)_{crit}$ . Above the critical mass-to-flux ratio the magnetic field cannot support the observed mass against gravitational collapse.

Inferring  $\lambda$  from observations is possible if the column density  $N$  and the magnetic field strength  $B$  can be determined such that:

$$\lambda = \frac{(M/\Phi)_{obs}}{(M/\Phi)_{crit}} = \frac{(mNA/BA)}{(1/2\pi\sqrt{G})} = 7.6 \times 10^{-21} \frac{N(H_2)}{B}, \quad (2)$$

where  $m = 2.8m_H$ , allowing for 10% He by number, with  $N(H_2)$  in  $\text{cm}^{-2}$  and  $B$  in  $\mu\text{G}$ .

Crutcher et al. (2004) estimated that the three cores they analysed had  $B_{pos} \sim 80 - 160 \mu\text{G}$  and  $\lambda \sim 1.9 - 2.6$ . When corrected downwards by a statistical factor of three for geometrical bias this showed that the magnetic field strength was such as to render each core slightly magnetically subcritical.

However, both Ward-Thompson et al. (2000) and Crutcher et al. (2004) pointed out that the offset between the core short axis and the magnetic field direction was not consistent with magnetically-regulated star formation models (e.g. Ciolek & Mouschovias 1998, and references therein). These models predict preferential collapse along the short axis of the core, yielding a field direction parallel to the short axis. This was explained as a projection effect in tri-

axial cores (Basu 2000; Ciolek & Basu 2004), and it was claimed that the data were consistent with the models.

All three of the prestellar cores previously mapped with the SCUBA polarimeter belong to the group of bright cores in the KWA survey. In this paper we present data for two more cores, L1498 and L1517B, which are somewhat less luminous. L1517B is a bright core and L1498 is in the intermediate group, although both lie near the borderline, and they are in fact quite similar. The goal is to examine whether the magnetic field morphology and/or strength change with submillimetre brightness, mass or evolutionary stage.

We describe the observational parameters in the next Section and present our data in Section 3. In Section 4 we apply the CF technique to the new data and calculate various physical parameters of the cores.

## 2 OBSERVATIONS

Submillimetre continuum observations at  $850 \mu\text{m}$  were carried out using SCUBA (Holland et al. 1999) on the JCMT on Mauna Kea, Hawaii, during the evenings of 1999 August 13–15 between the hours 01:30 and 09:30 HST (11:30–19:30 UT) and on the evenings of 2004 February 2–3 between the hours 17:30 and 01:30 HST (03:30–11:30 UT).

SCUBA was used with the SCUBAPOL (Greaves et al. 2003) polarimeter, which uses a rotating half-waveplate and fixed analyser. The waveplate is stepped through sixteen positions (each offset from the last by  $22.5^\circ$ ) and a Nyquist-sampled image (using a 16-point jiggle pattern) is taken at each waveplate position (Greaves et al. 2003). The observations were carried out whilst chopping the secondary mirror 120 arcsec in azimuth at 7 Hz and synchronously detecting the signal, thus rejecting sky emission.

The integration time per point in the jiggle cycle was 1 second, in each of the left and right telescope beams of the dual-beam chop. The total on-source integration time per complete cycle was 512 seconds. Two sources were observed, L1498 and L1517B, and the entire observing process described above was repeated 46 times for L1498 and 32 times for L1517B.

The instrumental polarisation (IP) of each bolometer was measured on the planets Mars and Uranus. This was subtracted from the data before calculating the true source polarisation. The mean IP was found to be  $0.93 \pm 0.27\%$ . It was found necessary to offset the pointing between repeated observations so that holes left by the exclusion of bolometers with significantly higher than average noise statistics could be filled in. The submillimetre zenith opacity for atmospheric extinction removal was determined by comparison with the 1.3-mm sky opacity (Archibald et al. 2002). The average  $850\text{-}\mu\text{m}$  zenith opacity was 0.28 during the 1999 observations and 0.19 during the 2004 observations, corresponding to a mean zenith transmission of 76 and 83% respectively.

## 3 RESULTS

Figures 1 and 2 show maps of the prestellar cores L1498 and L1517B. The greyscale and contours show the Stokes I (intensity) of the dust emission. The absolute calibration of

the intensity is not maintained through polarimetry observations. Therefore we simply show the contours as a fraction of the peak intensity and refer to previous observations to obtain the absolute intensity calibration and parameters derived therefrom. For example, KWA found peak flux densities of 120 and 170 mJy/beam and integrated flux densities of 2.3 and 2.6 Jy respectively for L1498 and L1517B at 850  $\mu$ m. We use these data below to calculate core masses and densities.

We note that there is a 180° ambiguity in the field direction, as two anti-parallel fields would generate the same polarisation. The correct mathematical term for such a vector with a 180° ambiguity is a ‘half vector’. Therefore, this is the term that we use. The half vectors in Figures 1 & 2 show the direction of the magnetic field in the plane of the sky. This is inferred from the assumption that the dust grains are magnetically aligned and that the magnetic field direction is orthogonal to the direction of polarisation (Davis & Greenstein 1951). Therefore the polarisation half vectors have been rotated by 90° to indicate the field direction.

The half vectors in Figures 1 & 2 are binned at 12 arcsec spacing to roughly match the JCMT beam FWHM of  $\sim$ 14 arcsec at 850  $\mu$ m. Only those half vectors with a signal-to-noise ratio  $\geq 2\sigma$  are plotted. This corresponds to a maximum position angle uncertainty of  $\pm 14^\circ$ . For each core the highest detection was found to be just under  $8\sigma$  and the mean half vector signal-to-noise ratio was  $\sim 4\text{--}5\sigma$ .

Note that, whenever we quote an error-bar on a polarisation half vector position angle measurement, we are quoting the observational error rather than the dispersion observed from one half vector to another. This error can be calculated for a single half vector from its signal-to-noise ratio, based on its stability as a function of time throughout the observations. This can be cross-checked using the known sensitivity of the instrument, the observing conditions and the total integration time. The error-bar for a group of half vectors can then be calculated from each half vector’s individual error-bar.

### 3.1 L1498

Figure 1 shows an intensity map of L1498 at 850  $\mu$ m as a greyscale with contours overlaid. Superposed on this are a series of polarisation half vectors which have been rotated by 90° to illustrate the magnetic field direction. The length of each half vector is proportional to the percentage polarisation observed. Looking first at the morphology of the core, we see an elongated core extending northwest to southeast, with a brighter peak at its northwestern end and a tail extending to the southeast. KWA also mapped L1498 at 850  $\mu$ m, but in photometric mapping mode only, and observed a slightly more rounded morphology.

The intensity map presented in Figure 1 is deeper and larger in extent than the previous map and shows that the chop direction chosen for the original map was almost parallel to the long axis of the core (the orientation of the core on these scales was not known at the time of the original observations). The chop function of the KWA data (see their section 5.4) caused an underestimate of the structure parallel to the major axis of the core and an offset in the apparent position angle of the core. It also led to an underestimate of

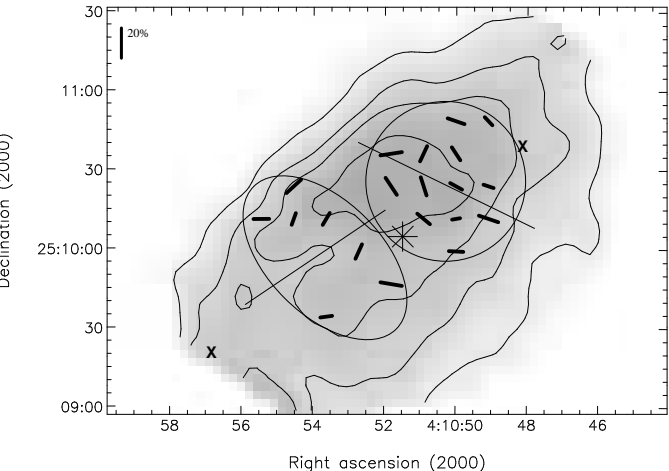


**Figure 1.** The prestellar core L1498 seen in submillimetre continuum dust emission at a wavelength of 850  $\mu$ m. The contours are at 40, 60, 80 & 90% of peak intensity. The polarisation half vectors have been rotated by 90° to show the magnetic field direction on the plane of the sky. The length of each half vector is proportional to the percentage polarisation. The ovals show groups of half vectors with roughly similar orientations and the line through each oval shows the approximate mean weighted PA of each group. The crosses mark the centres of integrated CCS emission observed by Lai & Crutcher (2000). The star marks the location of the CCS Zeeman observation undertaken by Levin et al. (2001).

the magnitude of the extended flux density. Correcting for the chop function takes L1498 to being a borderline ‘bright’ core, even more similar to L1517B.

The map of L1498 in Figure 1 shows an elliptical core with a position angle (PA) for the long axis of the extended emission of  $\sim 135^\circ \pm 5^\circ$ . The flux distribution is asymmetric along the long axis as mentioned above. The far-infrared maps made by the Infrared Space Observatory (ISO) of this region show that the L1498 core is at the northwestern end of a filament extending from the main cloud which lies to the southeast (Ward-Thompson, André & Kirk 2002).

The surface of this filament appears to be being heated by the inter-stellar radiation field (ISRF) and has a higher colour temperature than the interior of the core (Ward-Thompson et al. 2002). The PA of the major axis of the core seen in our new data is coincident with the PA of the filament seen in the ISO maps (c.f. figure 7 of KWA). The tail of emission seen in Figure 1 heading to the southeast of the core is the start of this filament.

However, there is an anti-correlation between the peak of the 850- $\mu$ m emission and the peak of integrated CCS and CS emission. The latter peaks towards the SE of the core (Tafalla et al. 2004; Lai & Crutcher 2000). Figure 8 of Lai & Crutcher (2000) shows what appears to be a CCS ring shape with a central depleted ‘hole’. The peaks of the CCS emission are shown as crosses in Figure 1.

We detect twenty polarisation half vectors across L1498 above the  $2\sigma$  cut-off. There appears to be a dramatic change in field direction from the half vectors in the brighter northwestern part of the core to those in the southeastern part. The two groups are shown encircled on Figure 1. In between there is a gap in the half vectors where presumably the two

different field directions compete and cancel the net polarisation.

The thirteen half vectors on the core peak have a weighted mean PA of  $64^\circ \pm 7^\circ$ , which is at an angle of  $19^\circ \pm 12^\circ$  to the PA of the short axis of the core. This alignment offset of the magnetic field to the orientation of the core short axis is similar to the  $\sim 20\text{--}30^\circ$  offset found in previous observations of prestellar cores (Ward-Thompson et al. 2000), as discussed in section 1 above.

The seven half vectors away from the core peak in the southeastern tail have a weighted mean PA of  $124^\circ \pm 6^\circ$  and are approximately parallel ( $11^\circ \pm 11^\circ$  offset) to the long axis of the core. This rotation of the magnetic field through  $60^\circ \pm 11^\circ$  is very marked and is most unusual. It has not been observed in a prestellar core before (Ward-Thompson et al. 2000). We note that the seven half vectors in the core's tail are coincident with the 'hole' in CCS emission discussed above, and with a region of anomalous velocity seen in  $\text{N}_2\text{H}^+$  (Tafalla et al. 2004).

However, we noted above that the tail to the southeast seen in Figure 1 is also seen in the ISO data to extend even further to the southeast, as a filament linking up to the rest of the cloud (see figure 7 of KWA). So it may be that the extended filament has a different B-field direction from the dense core at its head and that the two fields have essentially become decoupled. If that is the case, then it seems quite remarkable that the two fields have become so decoupled as to lie at such a large apparent angle to one another.

### 3.2 L1517B

The map of L1517B in Figure 2 shows a peak of emission with a tail that extends to the southwest. The composite ISO and SCUBA maps of KWA show that L1517B extends in a truncated filament northeast of the main L1517 cloud. The peak of submillimetre intensity is near the 'head' of this filament and the tail points back towards the main cloud. Hence it has a somewhat similar morphology and situation to L1498, with a core near the head of a filament.

However, there is also some evidence in the intensity map of Figure 2 that there is a slight extension of the filament to the north of the peak, and that the filament turns slightly. Furthermore, the ISO data also show some evidence for a twist in the filament just to the north of L1517B (see figure 7 of KWA). Hence we see that the elongated filament in which the peak sits turns slightly from its northern end to its southern part. This is illustrated in Figure 2 by a curved dashed line which follows the ridge of the filament.

We detected seventeen polarisation half vectors across L1517B above the  $2\sigma$  cut-off. They have a weighted mean PA of  $106^\circ \pm 7^\circ$ . However, the morphology of the half vectors does not at first appear to be a simple uniform pattern. They were split into three groups of similar orientation half vectors – the northern four half vectors (PA  $\sim 82^\circ \pm 6^\circ$ ), the middle nine half vectors (PA  $\sim 94^\circ \pm 6^\circ$ ), and the southern four half vectors (PA  $\sim 156^\circ \pm 5^\circ$ ) – as shown in Figure 2. There appears to be a progression in mean PA from the north to the south, indicating a change in the mean field direction.

The PA of the long axis of the filament was measured at the centre of each oval, and found to be  $15^\circ \pm 5^\circ$ ,  $35^\circ \pm 5^\circ$  and  $50^\circ \pm 5^\circ$  from north to south respectively. Therefore the

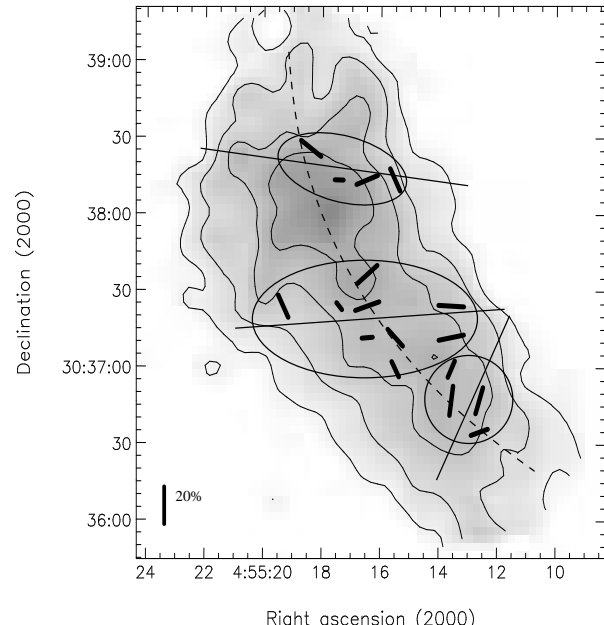


**Figure 2.** The prestellar core L1517B in submillimetre dust emission at  $850\text{ }\mu\text{m}$ . The contours are at 40, 60, 80 & 90% of peak intensity. The polarisation half vectors have again been rotated by  $90^\circ$  to show the plane-of-sky magnetic field direction. The ovals show groups of half vectors of similar orientation and the lines through the ovals show the approximate mean weighted PA of those half vectors. The dashed line shows the ridge of the larger filament in which the core is embedded.

angle between the field direction and the filament elongation axis is  $67^\circ \pm 11^\circ$ ,  $59^\circ \pm 11^\circ$  and  $75^\circ \pm 10^\circ$  from north to south respectively.

The mean of these is  $65^\circ \pm 6^\circ$ , and hence the mean of the offset from the short axis is  $25^\circ \pm 6^\circ$ , consistent with that seen in the core of L1498, and with previous observations of prestellar cores (Ward-Thompson et al. 2000). So we see that the field is simply following the twist in the filament and remaining at a roughly constant offset to it, as was seen before. However, we note that the sign of the offset flips in the south. This flip cannot be explained by the argument that this is simply a projection effect in a triaxial core, as suggested by the proponents of the magnetically regulated models (Basu 2000; Ciolek & Basu 2004).

## 4 DISCUSSION

We can use our measurements not only to map the orientation of the magnetic field, but also to estimate the strength of the field in the plane of the sky, using the CF method, as discussed in section 1 above. For this we need to measure the dispersion in the polarisation half vectors (corrected for dispersion caused by observational errors), and to compare this with the mass, density and non-thermal spectral linewidth in each core.

The densities of the cores were estimated by assuming that they are triaxial ellipsoids, with the line-of-sight axis being the mean of the other two axes. We use the continuum data of KWA to calculate the dust mass, and hence the total mass of each core. The conversion from total mass to mass of

Source	L1498	L1517B
Distance (pc)	140	140
Diameter (pc)	$0.04 \times 0.04$	$0.03 \times 0.02$
$M_{obs}$ ( $M_{\odot}$ )	$0.3 \pm 0.1$	$0.3 \pm 0.1$
$\bar{N}(H_2)$ ( $10^{22} \text{ cm}^{-2}$ )	$1 \pm 0.5$	$3 \pm 2$
$\bar{n}(H_2)$ ( $10^5 \text{ cm}^{-3}$ )	$1 \pm 0.5$	$6 \pm 3$
$\delta\phi$ ( $^{\circ}$ )	$40 \pm 7$	$30 \pm 5$
$B_{pos}$ ( $\mu\text{G}$ )	$10 \pm 7$	$30 \pm 10$
$\lambda_{obs}$	$8 \pm 5$	$7 \pm 4$
$\lambda_{corr}$	$3 \pm 2$	$2 \pm 1$
$M_{B,crit}$ ( $M_{\odot}$ )	$0.1 \pm 0.07$	$0.15 \pm 0.1$
$\Delta V$ ( $\text{km s}^{-1}$ )	$0.204 \pm 0.01$	$0.195 \pm 0.01$
$M_{\Delta V}$ ( $M_{\odot}$ )	$0.8 \pm 0.13$	$0.4 \pm 0.15$
$M_{B,vir}$ ( $M_{\odot}$ )	$0.9 \pm 0.2$	$0.55 \pm 0.25$
$M_{P,obs}$ ( $M_{\odot}$ )	$0.8 \pm 0.4$	$0.6 \pm 0.3$

**Table 1.** Calculated parameters of the prestellar cores L1498 and L1517B. For the distances we followed KWA. The sizes were measured from Figures 1 & 2. The masses  $M_{obs}$  and column densities  $\bar{N}(H_2)$  were estimated from the submillimetre photometric mapping of KWA. The volume densities  $\bar{n}(H_2)$  were calculated assuming that the line-of-sight dimension of each core was the mean of its other two dimensions. The half vector dispersion  $\delta\phi$  was corrected for the dispersion due to observational error. The plane-of-sky B-field strength  $B_{pos}$  was calculated from these parameters by the CF method. The ratio of the observed mass-to-flux ratio to the critical mass-to-flux ratio,  $\lambda_{obs}$ , was calculated from the mass and magnetic field strength, and corrected by a mean geometrical factor of 3 to produce the corrected value  $\lambda_{corr}$ . The critical mass that could be supported by the field  $M_{B,crit}$  was calculated from this. The linewidths  $\Delta V$  are from Tafalla et al. (2004). The (thermal plus nonthermal) virial mass  $M_{\Delta V}$  was calculated from the linewidth. The total virial mass  $M_{B,vir}$  was calculated by adding together  $M_{B,crit}$  and  $M_{\Delta V}$ . In both cases  $M_{B,vir}$  is larger than  $M_{obs}$ , although  $M_{obs}$  must be corrected for external pressure to obtain  $M_{P,obs}$ , which is seen to be consistent with  $M_{B,vir}$  in both cases (see text for discussion).

$H_2$  is made using the standard solar abundance of H. These values were calculated and are listed in Table 1.

The half vector dispersion  $\delta\phi$  was corrected for the dispersion due to observational error (see: Crutcher et al. 2004, for discussion).  $B_{pos}$  was calculated from these parameters by the CF method. The ratio of the observed mass-to-flux ratio to the critical mass-to-flux ratio,  $\lambda$ , was calculated from the mass and magnetic field strength, and corrected by a mean geometrical factor of 3, following Crutcher et al. (2004).

For L1498 we calculated the size, mass and density of the core peak only. To do this we measured the flux density in the northern circular aperture on Figure 1 using the KWA data. We corrected for the chop function along the long axis of the core, as discussed in section 3.1 above. We used this to calculate the column density and hence the mass. Similarly we only measured the half vector dispersion of the thirteen half vectors on the core peak, so as to exclude from our calculations the large turn of the apparent field direction from the core peak to the filamentary tail discussed in section 3.1 above.

Our calculations using the CF method give us a plane-of-sky magnetic field strength for L1498 of  $\sim 10 \pm 7 \mu\text{G}$ . This yields a geometrically-corrected ratio,  $\lambda_{corr}$ , of the observed to critical mass-to-flux ratios of  $3 \pm 2$ . Zeeman

measurements of the line-of-sight magnetic field strength in L1498 (Levin et al. 2001) were taken at the central position of the core, marked by a star on Figure 1. These gave a field strength of  $48 \pm 31 \mu\text{G}$  in the line of sight. These two numbers are comparable, to within errors, so we are not seeing the field at any particularly special angle. Adding the two components in quadrature gives a total field strength of  $49 \pm 33 \mu\text{G}$ . Hence we see that our geometrical correction factor of  $\sim 3$  is consistent to within the errors, and we therefore leave it unchanged to preserve comparability between the results for different cores. From our derived value of  $\lambda_{corr}$  we calculate the magnetic critical mass to be  $0.1 \pm 0.07 M_{\odot}$ .

For L1517B we calculated the half vector dispersion separately in each of the three ovals shown in Figure 2 above, and then took the weighted mean of the three dispersions. Thus we excluded any contribution to the dispersion from the large-scale twist in the magnetic field discussed in section 3.2 above. Hence the CF method yields a plane-of-sky magnetic field strength for L1517B of  $\sim 30 \pm 10 \mu\text{G}$ . This gives a geometrically-corrected ratio,  $\lambda_{corr}$ , of the observed to critical mass-to-flux ratios of  $2 \pm 1$ . We note that in both cores the half vector dispersion is greater than the recommended upper limit of  $25^{\circ}$  for finding accurate CF results (Ostriker, Gammie & Stone, 2001), so our values may be somewhat more uncertain as a result of this. We obtain a magnetic critical mass for L1517B of  $0.15 \pm 0.1 M_{\odot}$ .

Tafalla et al. (2004) observed L1498 and L1517B in multiple transitions of a range of nitrogen- and carbon-based molecules. They recorded respective mean intrinsic  $\text{N}_2\text{H}^+$  FWHM linewidths of  $0.204$  and  $0.195 \text{ km s}^{-1}$  respectively, as listed in Table 1. We note that these authors found the same linewidths for  $\text{NH}_3$ . They also found the non-thermal linewidths  $\Delta V_{NT}$  to be  $0.12$  and  $0.11 \text{ km s}^{-1}$  respectively, as used in the CF calculation above. These non-thermal linewidths are approximately a third to a half of those found for the three cores studied by Crutcher et al. (2004).

We used the total linewidths to calculate the (thermal plus non-thermal) virial masses of the cores,  $M_{\Delta V}$ , that could be supported virially by these linewidths, and found them to be  $0.8$  and  $0.4 M_{\odot}$  for L1498 and L1517B respectively. We list these in Table 1. We note that the mass able to be supported in this way is greater than the observed mass in each case.

The parameters listed in Table 1 show that L1498 and L1517B are rather similar in terms of their properties such as size, mass, density and velocity dispersion. Therefore, the fact that their field morphologies are very different from one another, as discussed in section 3 above, is somewhat surprising. Table 1 shows that both cores appear to exceed their critical mass-to-flux ratios by a factor of  $\sim 2\text{--}3$ . We also see that the (thermal plus non-thermal) virial mass,  $M_{\Delta V}$ , in each case is larger than the observed mass.

We can estimate the total virial mass,  $M_{B,vir}$ , (excluding the effects of external pressure) by adding together the (thermal plus non-thermal) virial mass,  $M_{\Delta V}$ , and the magnetic critical mass,  $M_{B,crit}$ . We find values of  $0.9$  and  $0.55 M_{\odot}$  respectively. We list these in Table 1. In both cases we see that the total virial mass,  $M_{B,vir}$ , is larger than the observed mass of the core.

In the foregoing we have simply calculated the masses in the regions for which we have measured the magnetic field strengths. However, we know from KWA that the total mass

of each core is greater than simply the mass of the central region. Hence we account for the extra mass by considering this as an external pressure acting on the central region in each case.

We can estimate this external pressure for a spherically symmetric core using the expression  $4\pi R^3 n_{ext} k T$ , where  $k$  is Boltzmann's constant,  $T$  is the core temperature (found from KWA),  $n_{ext}$  is the external surface density and  $R$  is the radius under consideration.  $n_{ext}$  was calculated by measuring the difference in mass between apertures of radii  $R$  and  $R + dr$  and assuming that this mass came from a shell of material of thickness  $dr$ . The density in this shell was found to be  $\sim 1 \times 10^5 \text{ cm}^{-3}$  for L1498 and  $\sim 3 \times 10^5 \text{ cm}^{-3}$  for L1517B. The value for L1498 is in fact consistent with a uniform density out to the maximum radius probed.

We can incorporate this, as a correction for external pressure, to our observed mass  $M_{obs}$ , to obtain  $M_{P,obs}$  (c.f. Ward-Thompson 2002; Ward-Thompson et al. 2006). We find that the additional pressure translates into an equivalent additional mass of 0.5 and 0.3  $M_\odot$  in L1498 and L1517B respectively. Adding these to  $M_{obs}$  we obtain values of  $M_{P,obs}$  of 0.8 and 0.6  $M_\odot$  in L1498 and L1517B respectively. These values are listed in Table 1. We estimate that the error-bars on these values could be as high as  $\sim 50\%$ , nevertheless we see that  $M_{B,vir} \sim M_{P,obs}$  for both cores, and thus both are consistent with being virialised.

These two cores appear somewhat different from the three cores studied by Crutcher et al. (2004), in that they have significantly lower non-thermal linewidths and magnetic field strengths. We commented above that the three cores previously studied (L1544, L183 & L43) were all in the 'bright' core category of KWA, whereas L1498 and L1517B studied here both lie near the border-line between the 'bright' and 'intermediate' cores of KWA. Therefore we postulate that perhaps we are seeing a trend for the denser 'bright' cores to have higher non-thermal linewidths and magnetic field strengths. In addition, for the denser cores thermal and non-thermal (including magnetic) support are approximately equal, while for the lower density cores, thermal support dominates.

## 5 CONCLUSIONS

We have mapped linearly polarized dust emission from the prestellar cores L1498 and L1517B at a wavelength of  $850 \mu\text{m}$  and used the measurements to determine the plane-of-sky magnetic field orientation in the cores. In L1498 we saw a magnetic field on the core peak that is offset from the core short axis by  $\sim 19^\circ \pm 12^\circ$ . To the southeast of the peak, in the filamentary tail, we saw that the magnetic field has rotated to lie almost parallel to the long axis of the filament. We hypothesised that the field in the core may have decoupled from the field in the filament that connects the core to the rest of the cloud. We used the CF method to measure the magnetic field strength in the core of L1498 and found it to be  $\sim 10 \pm 7 \mu\text{G}$ .

In L1517B we saw a more gradual turn in the field direction from the northern part of the core to the south. This appears to follow a twist in the filament in which the core is buried, with the field staying at a roughly constant offset of  $\sim 25^\circ \pm 6^\circ$  to the short axis of the filament. The CF method

was used to calculate the magnetic field strength in L1517B, which was found to be  $\sim 30 \pm 10 \mu\text{G}$ . Both cores were seen to be roughly virialised.

## ACKNOWLEDGMENTS

The James Clerk Maxwell Telescope is operated by the Joint Astronomy Centre on behalf of the Particle Physics and Astronomy Research Council of the United Kingdom, the Netherlands Organisation for Scientific Research, and the National Research Council of Canada. SCUBA and SCUBAPOL were built at the Royal Observatory, Edinburgh. The observations were carried out during observing runs with reference numbers M99BU38 and M04AU26. JMK acknowledges PPARC post-doctoral support at Cardiff University, as well as NSF post-doctoral support at the University of Illinois under grant NSF AST 02-28953, that enabled him to work on this project. DWT was on sabbatical at the Observatoire de Bordeaux whilst carrying out this work and gratefully acknowledges the hospitality accorded to him there. RMC received partial support from grant NSF AST 02-05810.

## REFERENCES

- Archibald E. N., et al., 2002, MNRAS, 336, 1
- Basu S., 2000, ApJ, 540, L103
- Basu S., Ciolek G. E., 2004, ApJ, 607, L39
- Benson P. J., Myers P. C., 1989, ApJS, 71, 89
- Beichman C. A., Myers P. C., Emerson J. P., Harris S., Mathieu R., Benson P. J., Jennings, R. E., 1986, ApJ, 307, 337
- Chandrasekhar S., Fermi E., 1953, ApJ, 118, 113 – CF
- Ciolek G. E., Mouschovias T. C., 1998, ApJ, 504, 280
- Crutcher R. M., Nutter D. J., Ward-Thompson D., Kirk J. M., 2004, ApJ, 600, 279
- Davis L. J., Greenstein J. L., 1951, ApJ, 114, 206
- Greaves J. S., et al., 2003, MNRAS, 340, 353
- Holland W. S., et al., 1999, MNRAS, 303, 659
- Jessop N. E., Ward-Thompson D., 2001, MNRAS, 323, 1025
- Kirk J. M., Ward-Thompson D., André P., 2005, MNRAS, 360, 1506 – KWA
- Lai S.-P., Crutcher R. M., 2000, ApJS, 128, 271
- Levin S. M., Langer W. D., Velusamy T., Kuiper T. B. H., Crutcher R. M., 2001, ApJ, 555, 850
- Ostriker E. C., Stone J. M., Gammie C. F., 2001, ApJ, 546, 980
- Tafalla M., Myers P. C., Caselli P., Walmsley C. M., 2004, A&A, 416, 191
- Ward-Thompson D., 2002, Science, 295, 76
- Ward-Thompson D., André P., Kirk, J. M., 2002, MNRAS, 329, 257
- Ward-Thompson D., Kirk J. M., Crutcher R. M., Greaves J. S., Holland W. S., André P., 2000, ApJ, 537, L135
- Ward-Thompson D., Nutter D., Bontemps S., Whitworth A., Attwood R., 2006, MNRAS, in press
- Ward-Thompson D., Scott P. F., Hills R. E., André P., 1994, MNRAS, 268, 276